Model of refractive-index changes in lithium niobate waveguides fabricated by ion implantation

Yi Jiang,* Ke-Ming Wang, Xue-Lin Wang, Feng Chen, Chuan-Lei Jia, Lei Wang, and Yang Jiao
School of Physics and Microelectronics, Shandong University, Jinan 250100, Shandong, People's Republic of China

Fei Lu
School of Information Science and Engineering, Shandong University, Jinan 250100, Shandong, People's Republic of China

(Received 18 September 2006; revised manuscript received 29 January 2007; published 3 May 2007)

A model is presented to explain the refractive-index changes in the ion-implanted $LiNbO_3$ waveguides that indicates that the lattice damage may be the main factor for the refractive-index changes. The model indicates that a slight enhancement may occur for the extraordinary refractive index in the ion-implanted $LiNbO_3$ waveguides with lattice damage ratios of less than 65%, and a maximum positive change ($\Delta n=0.0338$) occurs at a damage ratio of 33%. The model explains both the positive refractive-index changes observed in waveguides formed using 500 keV Si^+-ion implantation and the refractive-index changes observed in He^+-ion-implanted waveguides.

DOI: 10.1103/PhysRevB.75.195101 PACS number(s): 42.70.Mp, 61.80.Jh, 42.82.Et

I. INTRODUCTION

Implantation of light ions, such as He or H, has been a universal method for fabricating waveguide structures in most optical materials because of the high controllability and reproducibility of ion implantation.[1,2] This method will create an optical barrier with decreased refractive indices at the end of the ion track inside the substrate by nuclear energy deposition; consequently, a waveguide structure is produced between the air and the barrier. For He^+-implanted waveguides in lithium niobate ($LiNbO_3$), it is found that the extraordinary refractive index (n_e) experiences positive changes in the waveguide region.[3,4] Moreover, recent reports have demonstrated that the implantation of low-dose heavy ions may be used to fabricate nontunneling waveguides by increasing n_e.[5–7]

The investigation of the mechanism for the refractive-index changes seems to be a valuable and interesting work for both research and applications. Townsend *et al.* hypothesized that the positive refractive-index changes may have its origin in the changes of stoichiometry or phase.[1] Hu *et al.* suggested that the decreased spontaneous polarization may cause the increase of n_e.[8] Since the $LiNbO_3$ crystal lattice is composed of a network of oxygen octahedron (BO_6) and most of the optical properties of oxygen-octahedron ferroelectrics depend on the presence of BO_6 octahedron building blocks,[9] in this paper, we present a model to explain the refractive-index changes in ion-implanted $LiNbO_3$ waveguides based on the damage in the crystal lattice due to the ion implantation.

II. THEORY

As a ferroelectric crystal, refractive indices $n_{ij,0}$ in $LiNbO_3$ crystal suffer a refractive-index change due to the interaction of the quadratic electro-optic coefficients (g_{ij}) and the spontaneous polarization (P_S), which has the expression[10]

$$\frac{1}{n_{ij}^2}-\frac{1}{n_{ij,0}^2}=g_{ij}P_S^2. \tag{1}$$

According to the symmetry of $LiNbO_3$ and the direction of P_S, we have

$$\frac{1}{n_e^2}-\frac{1}{n_{e,0}^2}=g_{33}P_S^2$$

and

$$\frac{1}{n_o^2}-\frac{1}{n_{o,0}^2}=g_{13}P_S^2,$$

where n_{ij} (measured value) is the refractive index $n_{ij,0}$ after the interaction of g_{ij} and P_S.[11] $n_e=n_{33}$ is the extraordinary refractive index of $LiNbO_3$ crystal and $n_o=n_{13}$ is the ordinary refractive index. At a wavelength of 633 nm, the values are $n_e=2.2020$, $n_o=2.2860$ (measured using the prism-coupling method), $g_{33}=0.09\ m^4/C^2$, $g_{13}=0.02\ m^4/C^2$, and $P_S=0.71\ C/m^2$;[10] hence, we have $n_{e,0}=2.4933$ and $n_{o,0}=2.3586$ at 633 nm.

The Lorentz-Lorenz equation expresses a relation between the average refractive index $n=(n_o^2n_e)^{1/3}$, the molar polarizability a_M, and the molar volume V_M,[12,13]

$$(n^2-1)/(n^2+2)=a_M/V_M. \tag{2}$$

Differentiating Eq. (2), we get

$$dn=\frac{(n^2-1)(n^2+2)}{6n}\left(\frac{da_M}{a_M}+\frac{dV_M}{V_M}\right). \tag{3}$$

Integrating Eq. (3) on both sides, we have

$$\Delta n\approx\frac{(n^2-1)(n^2+2)}{6n}\left(\ln\frac{a_M+\Delta a_M}{a_M}+\ln\frac{V_M+\Delta V_M}{V_M}\right). \tag{4}$$

For light ions, the doses which are used to form waveguides in lithium niobate are around 10^{16} ions/cm^2; for heavier ions, the dose is around 10^{14} ions/cm^2. The anisotropy of $LiNbO_3$ refractive index was relative to the aniso-

tropy of its molar polarizability.[10] We ignore the doping effect in the implantation so that the changes of molar polarizability Δa_M do the main contribution to the change of refractive-index ellipse. We let

$$n_{ij,0} - n = \frac{(n^2-1)(n^2+2)}{6n} \ln \frac{a_M + \Delta a_{M,ij,k}}{a_M} \tag{5}$$

and obtain $\Delta a_{M,e}/a_M = 0.0389$ and $\Delta a_{M,o}/a_M = -0.0206$ for total damage ($n_{ij,0}=n$). If we assume that the values of refractive index in the $LiNbO_3$ after a large-dose implantation will reach an isotropy value n_i, then

$$n_i - n = \frac{(n^2-1)(n^2+2)}{6n} \ln \frac{V_M + \Delta V_{M,k}}{V_M}. \tag{6}$$

The value of n_i can be established from experiment and is about 2.1 (± 0.02),[14,15] so $\Delta V_M/V_M = 0.1230$ is obtained for full damage.

Considering that the changes of a_M and V_M should be relative to the damage done to the crystal lattice of $LiNbO_3$, we can simply assume a linear expression between the changes of a_M, V_M, and the lattice damage ratio k,

$$\frac{\Delta a_{M,ij,k}}{a_M} = \frac{\Delta a_{M,ij}}{a_M} k \quad \text{and} \quad \frac{\Delta V_{M,k}}{V_M} = \frac{\Delta V_M}{V_M} k.$$

Hence, the refractive-index changes under damage ratio k should have the following expression:

$$\Delta n_{e,k} \approx \frac{(n^2-1)(n^2+2)}{6n} \left[\ln\left(1 + \frac{\Delta a_{M,e}}{a_M} k\right) + \ln\left(1 + \frac{\Delta V_M}{V_M} k\right) \right], \tag{7}$$

$$\Delta n_{o,k} \approx \frac{(n^2-1)(n^2+2)}{6n} \left[\ln\left(1 + \frac{\Delta a_{M,o}}{a_M} k\right) + \ln\left(1 + \frac{\Delta V_M}{V_M} k\right) \right]. \tag{8}$$

.

Since the quadratic electro-optic coefficients are simply a function of crystal structure and the spontaneous polarization is a quadratic effect based on the crystal structure,[10] we assume a linear relation between them and obtain

$$g_{ij,k} = (1-k) g_{ij} \quad \text{and} \quad P_{S,k}^2 = (1-k) P_S^2.$$

When we apply these assumptions into Eq. (1), we have

$$n_{e,k} = \frac{1}{\sqrt{\left(\frac{1}{n_{e,0} - \Delta n_{e,k}}\right)^2 + g_{33} P_S^2 (1-k)^2}}, \tag{9}$$

$$n_{o,k} = \frac{1}{\sqrt{\left(\frac{1}{n_{o,0} - \Delta n_{o,k}}\right)^2 + g_{13} P_S^2 (1-k)^2}}. \tag{10}$$

Figure 1 shows the refractive indices of n_e [line (a)] and n_o [line (b)] calculated using Eqs. (9) and (10) versus the lattice damage ratio in the $LiNbO_3$ crystal. As can be seen, n_o continually decreases during the lattice damage, so only a barrier-type waveguide may be formed for n_o. On the other hand, the n_e would have a refractive-index enhancement when the lattice damage ratio is less than 65%. As line (a) indicates in the figure, n_e may reach a maximum positive change ($\Delta n = 0.0338$) at a damage ratio of 33%. The difference in the dependence of n_e and n_o on the damage ratio is due to the large value of g_{33} for n_e which leads to an increase of n_e for small values of k.

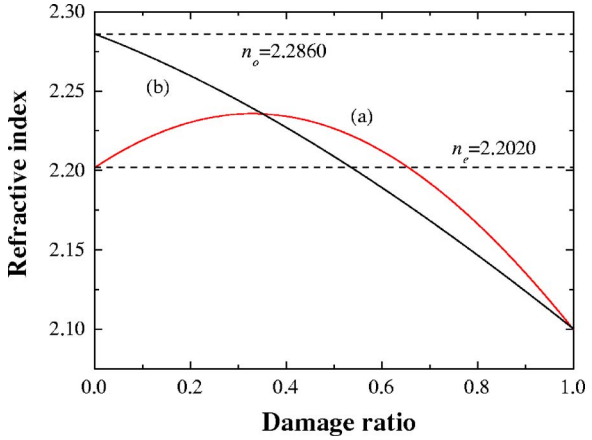

FIG. 1. (Color online) Refractive indices of n_e [line (a)] and n_o [line (b)] versus the lattice damage in the $LiNbO_3$ crystal. The dashed line represents the refractive indices of the virgin crystal.

III. EXPERIMENTAL DETAILS AND DISCUSSIONS

The samples we used were x-cut $LiNbO_3$ wafers with dimensions of $20 \times 5 \times 1.5$ mm^3 with the 5×1.5 mm^2 edges along the y direction. The 20×5 facets and the 5×1.5 mm^2 edges were optically polished and cleaned before the implantation. The room-temperature 500 keV Si^+-ion implantation was performed at the Institute of Semiconductors, Chinese Academy of Sciences. The implantation doses were 1×10^{14}, 3×10^{14}, and 5×10^{14} ions/cm^2. The ion beam was electrically scanned to ensure a uniform implantation over the samples. In order to avoid the channeling effect, the samples were titled 7° off of the beam direction. After the implantation, the samples were annealed in a furnace at a temperature of 230 °C for 30 min in dry oxygen to remove any unstable effects such as color center, stress, etc. Possible propagating modes of the planar waveguide were measured by the prism-coupling method with a model 2010 prism coupler (Metricon, NJ). A laser beam strikes the base of a prism, and hence, the laser beam was coupled into the waveguide region. A silicon photodetector was used to detect the reflected beam. The prism, waveguide, and photodetector were mounted on a rotary table so that the incident angle of the laser beam could be adjusted. The intensity of the reflected light was plotted as a function of incident angle, and a sharp drop in the intensity profile corresponds to a possible mode. This system has a refractive-index resolution better than 0.0001. An end-coupling-in and end-coupling-out system was set up to determine the property of the guide modes in the waveguide. A laser beam with a wavelength of 633 nm was used in the measurement. The lattice damage distributions of the implanted $LiNbO_3$ samples were estimated using

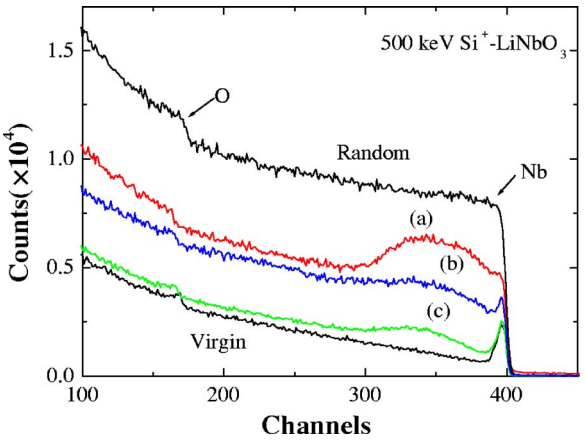

FIG. 2. (Color online) RBS/channeling spectra of 500 keV Si^+ ions implanted into the $LiNbO_3$ crystal with doses of (a) 5×10^{14} ions/cm^2, (b) 3×10^{14} ions/cm^2, and (c) 1×10^{14} ions/cm^2. The random and channel spectra of the virgin $LiNbO_3$ crystal are also presented.

the Rutherford backscattering spectroscopy/channeling (RBS/C) method at the 1.7 MV tandem accelerator of Shandong University with 2.1 MeV He^{2+} and a scattering angle of 165°.

Figure 2 shows the RBS/channeling spectra of the $LiNbO_3$ crystal after 500 keV Si^+-ion implantation. In order to obtain the lattice damage ratio from the spectra, a multiple-scattering dechanneling model based on the two-beam approximation[16] was applied, which is based on Feldman's procedure.[17] The damage ratio, which is defined as the ratio of displaced atoms N_D to the atom density N, is given by

$$\frac{N_D(t)}{N} = [x_2(t) - f_n(t)][1 - f_n(t)], \tag{11}$$

where $x_2(t)$ is the normalized yield from a disordered crystal at depth t, $f_n(t)$ is the fraction of the beam normal at depth t, and $N_D(t)/N$ is the ratio of displaced atoms at a depth t. $f_n(t)$ may be estimated from the multiple-scattering model:

$$f_n(t) = x_1(t) + [1 - x_1(t)]\exp\left[-\frac{\psi_c^2}{\Omega^2(t)}\right], \tag{12}$$

where $x_1(t)$ is the normalized yield from the perfect crystal at depth t, φ_c is the critical angle for channeling, and

$$\Omega^2(t) = \frac{\pi}{2}\psi_1^4 d^2 \int_0^t N_D(t')dt', \tag{13}$$

where $\varphi_1=(2Z_1Z_2e^2/Ed)^{1/2}$. Thus, $N_d(t)$ may be calculated by an iterative procedure. Starting from the surface $\Omega^2(0)=0$ and a defect density at the surface given by

$$\frac{N_D(0)}{N} = \frac{[x_2(0) - x_1(0)]}{[1 - x_1(0)]}, \tag{14}$$

the quality $N_D(t)/N$ is then calculated for each subsequent depth interval. The critical angle φ_c can be adjusted to make the damage profile satisfy the criterion that the damage density becomes zero just beyond the ion range. Figure 3 shows the damage ratio profiles calculated from the RBS/channeling spectra in the 500 keV Si^+-ion-implanted $LiNbO_3$ crystals with varying implant doses. The maximum damage ratios in the waveguide regions for implantation doses of 1×10^{14}, 3×10^{14}, and 5×10^{14} ions/cm^2 are about 20%, 33%, and 65%, respectively. Subsequently, we used Eq. (9) on the calculated damage profiles to get the extraordinary refractive-index profiles in the waveguide regions. The calculated refractive-index profiles are presented in Fig. 4, along with the smoothed line.

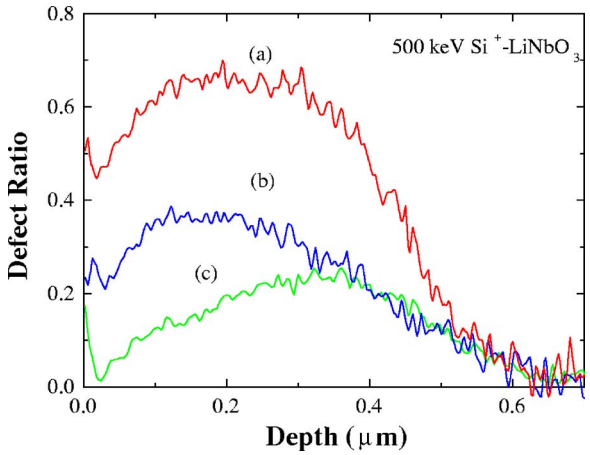

FIG. 3. (Color online) Damage profiles of the 500 keV Si^+-ion-implanted $LiNbO_3$ crystal with doses of (a) 5×10^{14} ions/cm^2, (b) 3×10^{14} ions/cm^2, and (c) 1×10^{14} ions/cm^2.

For our calculations, we consider a planar waveguide characterized by a refractive-index profile $n=n(x)$ which does not depend on y or z. The wave vector lies in the (y, z) plane, and we choose the z direction without loss of generality. All components of the electromagnetic field are shaped according to

$$F(t,x,y,z) = F(x)e^{-i\omega t}e^{i\beta z}, \tag{15}$$

where $\beta=n_{\text{eff}}k_0$ is defined as the propagation constant in the waveguide, n_{eff} is the efficient refractive index in the wave-

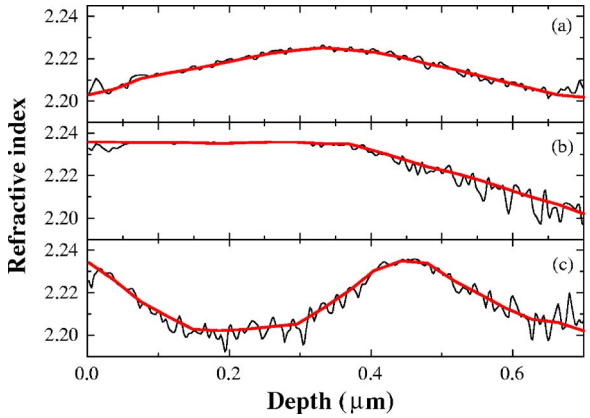

FIG. 4. (Color online) Refractive-index profiles (n_e) of the waveguide region in the $LiNbO_3$ crystal implanted using 500 keV Si^+ ions with doses of (a) 1×10^{14} ions/cm^2, (b) 3×10^{14} ions/cm^2, and (c) 5×10^{14} ions/cm^2. The smoothed lines are also presented.

TABLE I. Measured and calculated effective refractive indices of 500 keV Si^+-ion-implanted $LiNbO_3$ waveguides at doses from 1×10^{14} to 5×10^{14} ions/cm^2.

Effective refractive index	Dose of implanted Si^+ (ions/cm^2)		
	1×10^{14}	3×10^{14}	5×10^{14}
$n_{e,\text{measured}}$	2.2021	2.2081	2.2048
$n_{e,\text{calc}}$	2.2027	2.2085	2.2033

guide, and k_0 is the wave vector in a vacuum.

According to Maxwell's equations, we have

$$\frac{1}{k_0}\frac{d^2E}{dx^2} + n^2E = n_{\text{eff}}^2E, \tag{16}$$

or

$$\frac{1}{k_0}n^2\frac{d}{dx}n^{-2}\frac{d}{dx}H + n^2H = n_{\text{eff}}^2H, \tag{17}$$

where Eqs. (16) and (17) represent TE and TM modes, respectively.

By using a beam propagation method (BPM),[18] we can obtain the effective refractive indices or optical intensity profiles from the calculated refractive-index profiles. The calculated effective refractive indices of the waveguides formed by 500 keV Si^+-ion implantation are shown in Table I. As one can see, the calculated values have a difference of less than 0.0015 with the measured ones.

Since the method of end coupling has proven to be a direct way to determine the waveguide index profile, we also measured near-field optical intensities of the formed waveguides and compared them with the ones simulated using the BPM method from the calculated refractive-index profiles. Figure 5(a) shows the calculated near-field optical intensity of the waveguide with the refractive-index profile determined in Fig. 4. Figures 5(b)–5(d) show the comparison between the near-field optical intensity of experimental values and the values simulated from the calculated waveguide refractive-index profile. As it shows, the experimental values have an agreement of better than 90% with the calculated values.

IV. SIMULATIONS OF REFRACTIVE-INDEX CHANGE IN He^+-IMPLANTED $LiNbO_3$ WAVEGUIDES

He^+-implanted $LiNbO_3$ waveguides have proven to be a valuable method to form a waveguide structure in $LiNbO_3$. Zhang *et al.* had reported a "strange" mode in 2.5 MeV He^+-implanted $LiNbO_3$ waveguides which indicated a waveguide structure beyond the optical barrier.[19] In this case, a positive refractive-index change may occur in both sides of the optical barrier. Recently, Rams *et al.* also reported positive refractive-index changes in He^+-implanted $LiNbO_3$ waveguides. In the results they reported, they formed $LiNbO_3$ waveguides with only positive refractive-index change in He^+-implanted $LiNbO_3$ waveguides.[20] We use transport of ions in matter (TRIM'98) code[21] to simulate the 2.5 MeV He^+-implantation process and assume the normalized vacancy profile as the damage profile caused by ion implantation. According to the doses reported in Ref. 20, we used 10% of the normalized vacancy profile as the damage profile at low dose (dashed line in Fig. 6) and full for damage profile of high dose (solid line). By applying Eq. (9), the possible refractive-index profiles in the He^+-implantation $LiNbO_3$ waveguides at high and low doses are calculated and shown in Fig. 7. The dashed lines represent the refractive indices of the virgin $LiNbO_3$ crystal. For high doses, positive refractive-index changes occurred for the extraordinary refractive index in both sides of the optical barrier. These results are consistent with those measured in Ref. 20. For the ordinary refractive index, only negative refractive-index

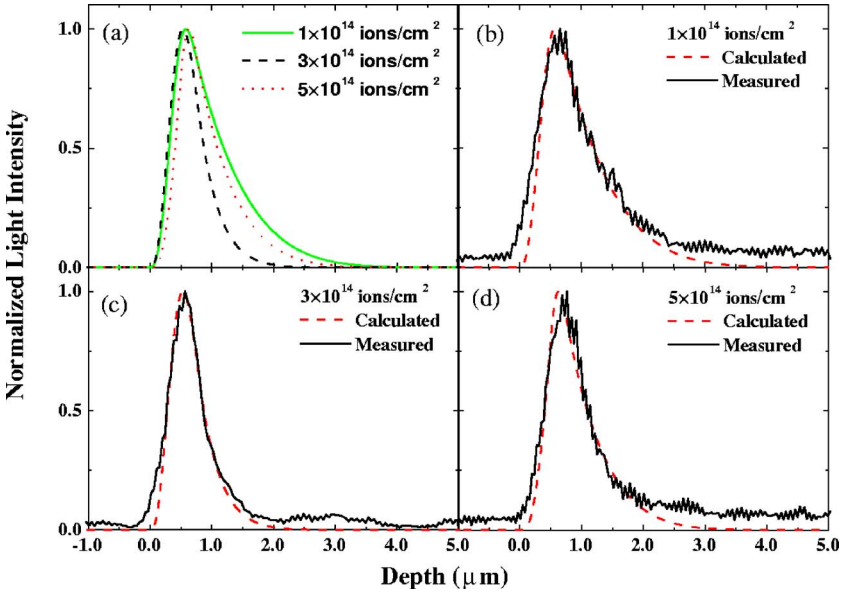

FIG. 5. (Color online) Comparison of the near-field optical intensity of experimental values to the calculated values. (a) indicates the difference between the calculated near-field optical intensities of different doses and (b), (c), and (d) is the comparison between the experimental values and the calculated values for doses of 1×10^{14} ions/cm^2, 3×10^{14} ions/cm^2, and 5×10^{14} ions/cm^2, respectively.

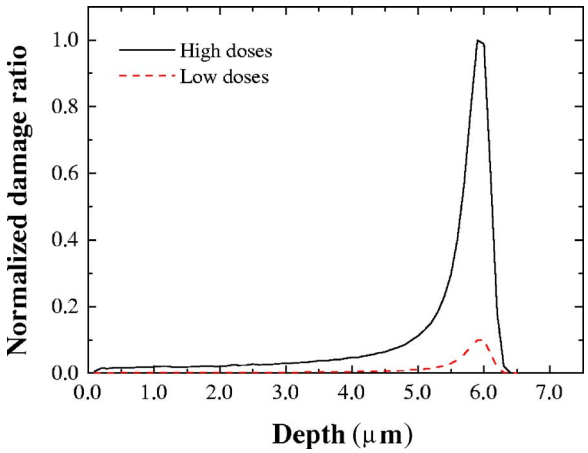

FIG. 6. (Color online) Normalized damage ratio of the 2.5 MeV He^+-ion-implanted $LiNbO_3$ crystal with a high dose (solid line) and a low dose (dashed line). The damage ratios were simulated using TRIM'98 code.

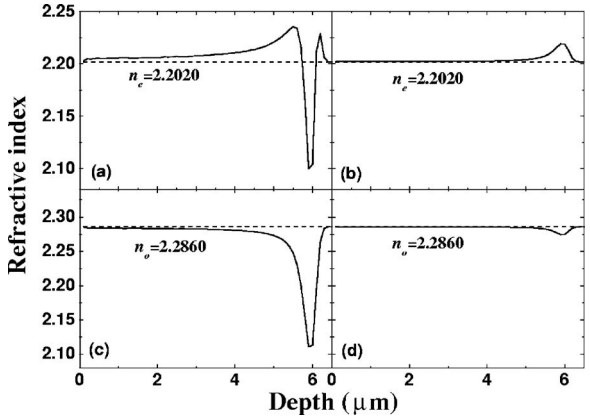

FIG. 7. Calculated refractive-index profiles of 2.5 MeV He^+-ion-implanted $LiNbO_3$ waveguides by assuming the vacancy profile simulated by TRIM'98 code as the lattice damage profile. Profiles (a) and (c) correspond to the normalized vacancy profile and (b) and (d) correspond to 10% of the normalized vacancy profile. The refractive indices of the virgin $LiNbO_3$ crystal are also presented.

changes occurred. It should also be noted that for low doses, only positive refractive-index changes occurred to the extraordinary refractive index [Fig. 7(b)], and only negative refractive-index changes occurred to the ordinary refractive index [Fig. 7(d)]. These results well explained the refractive-index changes observed in Ref. 20. Nevertheless, experimental confirmation for the fit of the calculated and measured effective refractive indices in these cases is still needed.

V. CONCLUSION

In this work, we have presented a model for explaining the refractive-index changes observed in ion-implanted lithium niobate waveguides. The model provides evidence that damage in the crystal lattice may be responsible for the refractive-index changes. We have shown that the effective refractive indices measured and those calculated using this model are in good agreement. The model was also applied to explain the waveguide formed by He^+-ion implantation. More experimental verification of the model is necessary, and we are currently carrying out research to accomplish this.

ACKNOWLEDGMENTS

The authors would like to thank Hairui Xia for the discussions on the $LiNbO_3$ structures and Peng Qi for the discussions on the ferroelectric theory. This work was supported by the National Natural Science Foundation of China (Grants No. 10575067 and No. 10475052).

*Electronic address: sdujy@mail.sdu.edu.cn

[1] P. D. Townsend, P. J. Chandler, and L. Zhang, *Optical Effects of Ion Implantation* (Cambridge University Press, Cambridge, UK, 1994).
[2] D. Fluck, P. Günter, R. Irmscher, and Ch. Buchal, Appl. Phys. Lett. **59**, 3213 (1991).
[3] P. J. Chandler, L. Zhang, J. M. Cabrera, and P. D. Townsend, Appl. Phys. Lett. **54**, 1287 (1989).
[4] S. M. Mahdavi, P. J. Chandler, and P. D. Townsend, J. Phys. D **22**, 1354 (1989).
[5] Gloria V. Vázquez, J. Rickards, G. Lifante, M. Domenech, and E. Cantelar, Opt. Express **11**, 1291 (2003).
[6] G. G. Bentini, M. Bianconi, M. Chiarini, L. Correra, C. Sada, P. Mazzoldi, N. Argiolas, M. Bazzan, and R. Guzzi, J. Appl. Phys. **92**, 6477 (2002).
[7] J. Olivares, G. García, A. García-Navarro, F. Agulló-López, O. Caballero, and A. García-Cabañes, Appl. Phys. Lett. **86**, 183501 (2005).
[8] H. Hu, F. Lu, F. Chen, B. R. Shi, K. M. Wang, and D. Y. Shen, Appl. Opt. **40**, 3759 (2001).
[9] S. H. Wemple, M. DiDomenico, and I. Camlibel, Appl. Phys. Lett. **12**, 209 (1968).
[10] M. DiDomenico and S. H. Wemple, J. Appl. Phys. **40**, 720 (1969).
[11] R. C. Miller and A. Savage, Appl. Phys. Lett. **9**, 169 (1966).
[12] H. Åhlfeldt, J. Webjörn, P. A. Thomas, and S. J. Teat, J. Appl. Phys. **77**, 4467 (1995).
[13] T. Mitsui, I. Tatsuzaki, and E. Nakawura, *An Introduction to the Physics of Ferroelectrics* (Gordon and Breach, New York, 1974).
[14] G. L. Destefanis, J. P. Gailliard, E. L. Ligeon, S. Valette, B. M. Farmery, P. D. Townsend, and A. Perez, J. Appl. Phys. **50**, 7898 (1979).
[15] Chuanlei Jia, Yi Jiang, Xuelin Wang, Feng Chen, Lei Wang, and Keming Wang, J. Appl. Phys. **100**, 033505 (2006).
[16] E. Bøgh, Can. J. Phys. **46**, 653 (1968).

[17] K. Sato, Y. Fujino, S. Yamaguchi, H. Naramoto, and K. Ozawa, Nucl. Instrum. Methods Phys. Res. B **47**, 421 (1990).
[18] L. Thylen, Numer. Simul. and Anal. Guided-Wave Opt. Optoelectron. **3**, 20 (1989).
[19] L. Zhang, P. J. Chandler, and P. D. Townsend, J. Appl. Phys. **70**, 1185 (1991).
[20] J. Rams, J. Olivares, P. J. Chandler, and P. D. Townsend, J. Appl. Phys. **87**, 3199 (2000).
[21] J. F. Ziegler, J. P. Biesack, and U. Littmark, *Stopping and Ranges of Ions in Matter* (Pergamon, New York, 1985).